Dielectric Characterization of a Nanofiltration Membrane in Electrolyte Solutions: Its Double-Layer Structure and Ion Permeation

Kongshuang Zhao* and Yuhong Li

Department of Chemistry, Beijing Normal University, Beijing 100875, China

Received: April 25, 2005; In Final Form: December 22, 2005

Dielectric spectroscopy (DS) was applied to a nanofiltration (NF) membrane to detect its double-layer structure and ion permeation. Dielectric measurements were carried out on the systems composed of the NF membrane NTR7450 and dilute solutions of eight electrolytes, LiCl, NaCl, KCl, NH_4Cl, $MgCl_2$, $CaCl_2$, $BaCl_2$, and $CuCl_2$. Two relaxations were observed in the frequency range from 40 Hz to 4 MHz for each system. On the basis of characteristics of the dielectric spectra and the Maxwell−Wagner interfacial polarization theory, the low-frequency relaxation was attributed to inhomogeneity of the membrane structure itself, whereas the high-frequency relaxation was attributed to interfacial polarization between the membrane and the solution. A multiphase dielectric model previously developed by one of the authors and co-workers was adopted to present systems to analyze the dielectric spectra, and electric parameters, i.e., capacitance and conductance, of the two layers composing the membrane were obtained. The electric properties estimated for the two layers were different and changed with the environment in a different manner. Further analyses suggest that the two layers had a different separation mechanism due to their difference in materials, looseness, and fixed charge content. The fixed charge density of one layer was estimated, and the ion permeation difficulties in both layers was compared. This research revealed that DS was by far an effective method to obtain detailed electric parameters about the inner multilayer structure of the NF membrane and to elucidate separation mechanisms of each layer.

1. Introduction

Nanofiltration (NF) membranes, which possess nanoscale pores and are charged weakly in general, have been widely used for liquid-phase separation recently. To extend NF's applicability, much research has been carried out to synthesize membranes of new materials or complex structures. Meanwhile, influences of membrane material and structure on its separation efficiency have attracted substantial attention.[1,2]

Among various separation processes, NF usually shows intermediate characteristics between ultrafiltration and reverse osmosis. Reverse osmosis membranes often have compact inner structure, and the dielectric exclusion effect, which is caused by different dielectric constants between the membrane material and the bulk solution, hinders transport of ions through the membrane. By comparison, the porous ultrafiltration membranes are usually more permeable to solvents; however, fixed charges on membrane polymer chains result in Donnan exclusion (i.e., electrostatic repulsion between fixed charges and coions in the solution) and make the membrane permselective with respect to ion size and charge. For NF membranes, because of their composite structure, separation mechanisms for reverse osmosis or ultrafiltration may operate simultaneously and influence each other, complicating the investigation of the NF processes.[3,4]

Although electron microscopy such as scanning electron microscopy (SEM), X-ray photoelectron spectroscopy (XPS), atomic force microscopy (AFM), etc., may give the surface morphology of dry membranes,[5−7] it cannot show the characteristics of the membranes under working conditions (e.g., soaked in solutions). It is these characteristics that are more closely related to membrane performance and the separation mechanism. Two other methods—measuring membrane potential and measuring salt permeability[4,8]—can be used to study membranes in the humid state, but both methods only give information on properties or the behavior of the whole membrane, but are incapable of detecting the inner structure of the membranes.

Dielectric spectroscopy (DS), as a noninvasive method and being especially sensitive to the heterogeneous system, has been successfully used in many fields including chemistry, biology, and materials,[9−14] and is shown to be valuable in studying the properties of membranes in the working state. In practical separation processes, membranes and aqueous solutions (or other liquids) form heterogeneous systems containing multiple phases, where Maxwell−Wagner interfacial polarization concept and theoretical formulas are suitable to analyze the dielectric spectra. A number of studies on the theory or on the behavior of different types of membrane−solution systems have been reported.[15−20] Most of these studies took the membranes as a homogeneous phase, or only explored special phenomena at the membrane−solution interface, such as water splitting and concentration polarization.[15−19] Coster et al. have studied inner structures of lipid bilayer membranes and other artificial polymer membranes in solution by the impedance spectroscopy method, and proposed sufficient theoretical explanations on the mechanisms of relaxations.[20,21] However, their studies mainly concentrated on relaxations at relatively low frequencies (ranging from 10^{-4} to 100 Hz). Zhao and co-workers have developed the dielectric

* Address correspondence to this author. E-mail: zhaoks@bnu.edu.cn. Phone: +86-010-588-08283. Fax: +86-010-588-05562.

10.1021/jp052154c CCC: $33.50
Published on Web 01/26/2006

model of the spliced layer structure and studied the corresponding systems,[15,17] but the focus of the studies was concentrated on some properties of the whole membrane and of the solution, or the behavior of the membrane in response to altered environment. In this work, however, our main objective is to study the nonuniformity of the membrane itself and to obtain more information about the complicated systems by DS.

Permittivity and conductivity, as two important parameters involved in DS, have close correlations with the constituent materials and their structures, as well as the ion transport in each phase of the heterogeneous system. For the NF membrane in separation processes, these two aspects are the origin and the result of separation mechanisms, respectively; therefore it is suitable to probe the relationship of the membrane inner structure and its separation mechanisms or efficiency by means of DS.

In this paper, dielectric responses of an NF membrane NTR7450 in dilute solutions of eight respective electrolytes were measured. The unique behavior of the measured systems was interpreted, and the relaxation mechanism was discussed in terms of Maxwell−Wagner theory. On the basis of the results, a dielectric model describing the nonuniformity of the membrane was proposed to analyze the dielectric spectra, and parameters on electric properties of each membrane layer were obtained and explained. Furthermore, the separation mechanisms of each layer in the membrane were discussed according to the principles of dielectric exclusion and Donnan equilibrium. The proposed spliced dielectric model is also expected to be useful for other fields.

2. Theoretical Aspects

2.1. Theoretical Background of Interfacial Polarization. For a heterogeneous system comprised of an artificial membrane and solutions at both sides, the dielectric behavior can be readily understood from the viewpoint of Maxwell−Wagner interfacial polarization theory. The membrane and solution domains have different permittivity ϵ and conductivity κ. When an electric field is applied to the system, spatial charges accumulate on the interfaces and produce an inductive field to keep the continuity of the electric current, similar to that in the multilayer capacitor. Generally, for planar heterogeneous systems having n dielectric slabs with different ϵ and κ, where n denotes the number of slabs, if only the following condition is satisfied, $n - 1$ relaxation processes with different characteristic relaxation time would be observed:[22,23]

$$\frac{\epsilon_1}{\kappa_1} \neq \frac{\epsilon_2}{\kappa_2} \neq \cdots \neq \frac{\epsilon_i}{\kappa_i} \neq \cdots \neq \frac{\epsilon_n}{\kappa_n} \quad (1)$$

This relation was confirmed by many experimental and theoretical studies, and was also found to hold in many practical membrane−solution systems of previous works, especially in systems with two or three layers,[9,24,25] although the number of dielectric relaxations observed for dispersed systems with n phases is sometimes less than $n - 1$.

In addition, electric circuit models are widely used in impedance or dielectric spectroscopy research. The electric property of one phase is described by a parallel connection of a capacitor and a resistor, and a serial connection of each phase in the system forms the equivalent circuit model to simulate the whole system. One of the authors and co-workers have proved the rationality of the phenomenological circuit model in previous studies:[26] the formula derived from electrostatic law is equivalent to that from a series combination of three lumped capacitance−conductance circuit models, and some experimental results observed in the terlamellar dielectric are shown to confirm the theoretical formulation proposed.

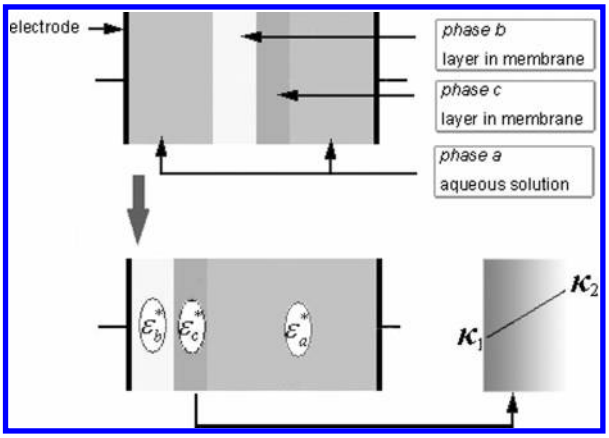

Figure 1. Dielectric model for the membrane−solution system. Schematic diagram of the measured system (upper) and its equivalent dielectric model (lower). The system is composed of three phases with different complex permittivity, that is, aqueous solutions (phase a), ϵ_a^*, layers in the membrane (phases b and c), ϵ_b^* and ϵ_c^*, respectively. Conductivity of phase c is linearly distributed.

It should be noted that the dielectric spectra expected from equivalent circuit models are simply represented by the sum of relaxations with a single relaxation time (i.e., Debye-type relaxation), whereas actual systems show much broader spectra with a distribution of relaxation time. Such broad spectra often trace circular arcs in complex plane plots. This phenomenon is very common when the dielectric slabs, arranged layer by layer, have a slight difference in electric property, because the relaxations due to different interfaces appear at close frequencies and overlap each other. Therefore, it is inadequate to describe dielectric spectra of these actual membrane−solution systems with the electric circuit model.

2.2. Dielectric Model for the Present Problem. In this work, dielectric measurements on the solution−membrane−solution systems gave two remarkable relaxations, as shown in Figures 2 and 3, indicating that there were at least three phases in the systems, according to the above discussions. Regarding the current measuring systems, the solutions at both sides of the membrane were considered as one phase because they contain identical electrolyte of the same concentration. Therefore the other two phases in the system were ascribed to the double-layer structure of the membrane, which is in agreement with the common recognition that NF membranes have a layered structure.

The complex plan plots for the high-frequency relaxations in each spectrum are perfect semicircles (shown at the left in Figure 3), whereas the low-frequency relaxations are arcs. As has been pointed out, semicircles represent Debye-type relaxations, which have a simplex relaxation mechanism. For the present system, these high-frequency relaxations could be considered to be caused by interfacial polarization between the entire membrane and the solution, because the membrane is much more insulating than the solution. Therefore the low-frequency relaxation represents the difference between the two layers in the membrane, and the distribution of relaxation time indicates that this difference is not prominent or there is a seriate transformation in the membrane electric property.

On the basis of the above analysis, a dielectric model was presented, as shown in Figure 1. The measured system is composed of three phases with different complex permittivity ϵ^* or complex capacitance C^*. The solutions are considered as

phase a, with capacitance C_a and conductance G_a. The NF membrane is considered to be two layers. One layer has homogeneous permittivity and conductivity, identified as phase b with capacitance C_b and conductance G_b. The other layer, phase c, has a homogeneous permittivity ϵ_c, but a linear distribution in conductivity in the direction perpendicular to the membrane surface, which is considered as the cause of relaxation time distribution in the low-frequency range. The conductivity of this layer is κ_1 at the side contacting phase *b*, and κ_2 at the side facing the solution. This treatment is based on the postulate that permittivity is mainly determined by the constituent material, while conductivity correlates more with the detailed inner structure of the membrane. Probably because of the nonuniformity in polymer looseness caused during membrane preparation, or because of the different environmental conditions on the two sides of this layer, ion permeation and transport in different depths of the membrane is different, which results in the distribution of membrane conductivity. However, the rationality of this model should be proved by the result of the dielectric analysis.

The mathematical treatment for this model is based on the principle that complex capacitance of a multilayer system is a serial combination of the complex capacitance of each layer. With respect to the conductivity distribution in phase *c*, the theoretical formulas, previously proposed by one of the authors for describing dielectric behavior of concentration polarization arising at membrane−solution interfaces, were adopted to solve the present problem.[27,28] In this way, capacitance and conductance of phase c are expressed by:

$$C_c(f) = \frac{S(\kappa_2 - \kappa_1)}{t} \frac{B/\omega}{A^2 + B^2} \tag{2}$$

and

$$G_c(f) = \frac{S(\kappa_2 - \kappa_1)}{t} \frac{A}{A^2 + B^2} \tag{3}$$

where t is thickness of phase c. $\omega = 2\pi f$, the angular frequency of the applied ac electric field. A and B are parameters introduced to facilitate the calculation, and are expressed as functions of ϵ_c, κ_1, and κ_2:[15,27]

$$A = \frac{1}{2} \ln\left(1 + \frac{(\kappa_2/\kappa_1)^2 - 1}{(1 + (\epsilon_c\epsilon_v/\kappa_1)^2\omega^2}\right) \tag{4}$$

and

$$B = \tan^{-1}\frac{(\kappa_2 - \kappa_1)\omega\epsilon_c\epsilon_v}{(\omega\epsilon_c\epsilon_v)^2 + \kappa_2\kappa_1} \tag{5}$$

where $\epsilon_v = 8.8542 \times 10^{-12}$ F·m^{-1}, permittivity of the vacuum. It can be seen from eqs 4 and 5 that the values of capacitance and conductance of phase c depend on the frequency of the applied electric field.

By dielectric measurements, we obtain complex capacitance $C(f)^*$ of the entire system, which contains two variables, capacitance $C(f)$ and conductance $G(f)$, both depending on frequency f:

$$C(f)^* = C(f)' - jC(f)'' = C(f) + \frac{G(f)}{j2\pi f} \tag{6}$$

The relationship between the entire system's complex capacitance and the constituent phases' is expressed by

$$\frac{1}{C(f)^*} = \frac{1}{C_a^*} + \frac{1}{C_b^*} + \frac{1}{C_c(f)^*} \tag{7}$$

The dielectric spectrum of the system can be calculated with eqs 2−7 by introducing values for the electric parameters (capacitance and conductance or permittivity and conductivity) for each phase.

2.3. Analyzing Method for Inner Parameters of the Membrane. To acquire the values of electric parameters of each phase, the least-squares method is employed to analyze the dielectric spectra, based on eqs 2−7. The best fitting is acquired when ξ reaches a minimal value. ξ is expressed as

$$\xi = \sum_{i=1}^{N}[(C'_{si} - C'_{ei})^2 + (C''_{si} - C''_{ei})^2] \tag{8}$$

where $N = 80$, the number of the applied frequencies; subscript *s* denotes calculated values, and *e* denotes experiment data.

To simplify the curve-fitting procedure, the variable parameters should be as few as possible. Since the capacitance and conductance of the solution, C_a and G_a, are obtained from measuring the solution in the same cell without membrane, those parameters are given. In consequence, the fitting gives the values of C_b, G_b, C_c, G_1, and G_2, where C_c is named as apparent capacitance of phase c, expressed by the equation of $C_c = \epsilon_v\epsilon_c S/t$, with definite values independent of frequency, differing from $C_c(f)$. If the thickness t of phase c is obtained, permittivity of phase c (ϵ_c) can be calculated readily. On the other hand, G_1 and G_2 are the conductance of phase c if we assume conductivity of phase c is as uniform as κ_1 or κ_2. That means, κ_1 and κ_2 could then be calculated with the following equations, if the thickness of phase c (t) is known:

$$\kappa_1 = G_1\frac{t}{S} \tag{9a}$$

and

$$\kappa_2 = G_2\frac{t}{S} \tag{9b}$$

These parameters will play an important role in discussing the two membrane layers' separation performance and mechanism.

3. Experimental Section

3.1. Pretreatment of the Membrane. The membrane used in this work was a composite NF membrane, NTR7450, which was kindly supplied by Nitto Denko Co. Japan. This membrane has a typical double-layer structure. The two layers in the membrane are composed of polyester and sulfonated polyether sulfone, respectively. The thickness of the membrane fully swollen in electrolyte solution was measured with a micrometer at about 120 μm. To remove impurities, the membrane was immersed in ethanol for 20 min, rinsed repeatedly with distilled water, immersed in distilled water for 24 h, and finally dried under room temperature. The whole membrane was cut into 8 pieces of the same size, which were subjected to dielectric measurements.

3.2. Dielectric Measurement. A precise impedance analyzer Agilent 4294A, whose basic impedance accuracy is ±0.08%, was employed in this work. A sample membrane was sand-

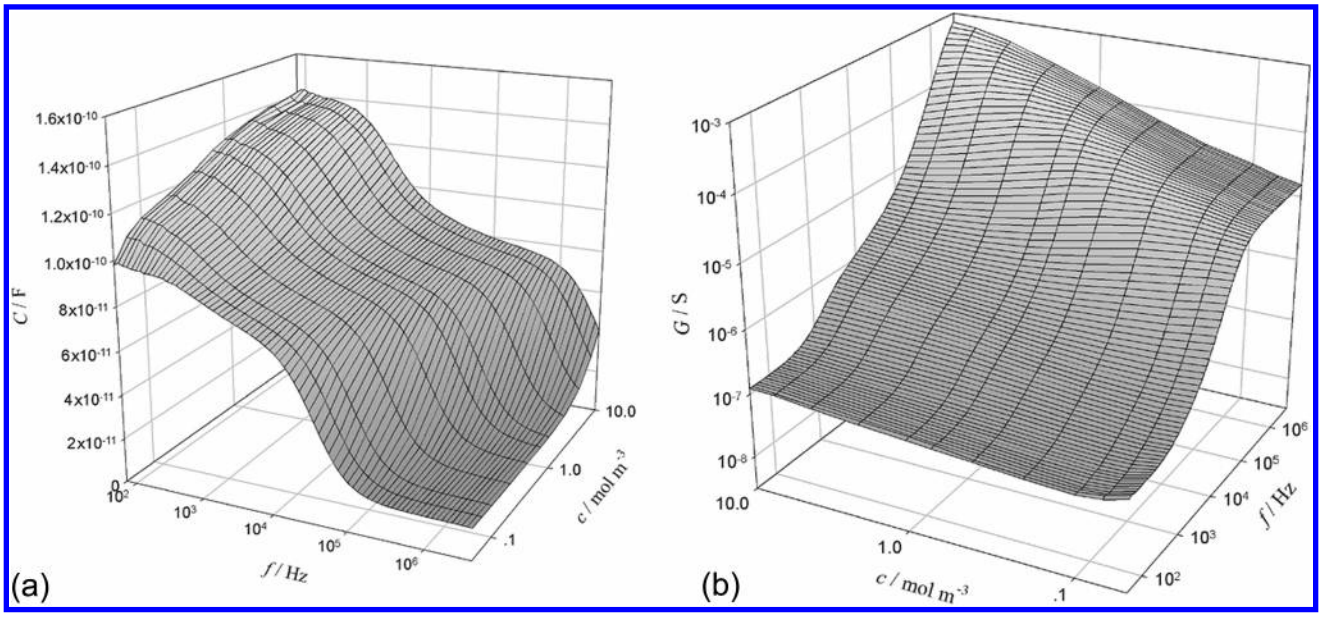

Figure 2. Dielectric spectra for the system composed of NF membrane and LiCl solutions. Capacitance (a) and conductance (b) vs frequency and bulk concentration.

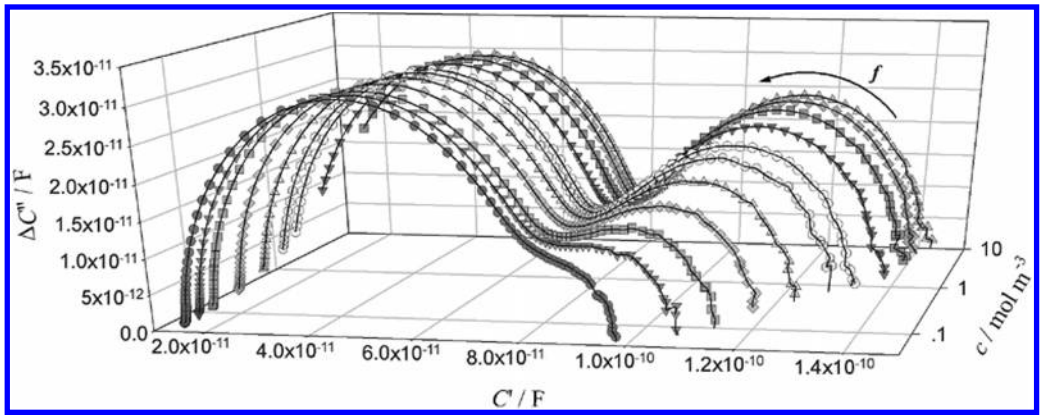

Figure 3. Complex plan plots of complex capacitance for the dielectric spectra of the system with NF membrane in LiCl solutions, in which $\Delta C'' = (G(f) - G_1)/2\pi f$, and G_1 is the low-frequency limit of conductance.

wiched between a pair of cylindrical chambers, which were filled with the same electrolyte solution, as shown in Figure 1 and described elsewhere.[17,26] The electrodes attached in the chambers form a parallel plate capacitor with an area (S) of 3.14 cm^2. The cell constant (S/L) is 2.414 cm, and L is the distance between the two electrodes. Prior to dielectric measurement, the dry membranes were immersed in solutions with the lowest concentration for 1 day to dispel the air in the membrane matrix and let the membrane swell to the largest extent. The cell systems with each piece of the membrane in eight respective electrolyte solutions were measured over a 40 Hz to 4 MHz frequency range, 80 points logarithmically spaced, by means of Agilent 4294A controlled by a personal computer. The data of a complete spectrum for one membrane−solution sample system were collected in about 50 s. The amplitude of the alternate voltage was 0.1 V. The electrolytes used were LiCl, NaCl, KCl, NH_4Cl, $MgCl_2$, $CaCl_2$, $BaCl_2$, and $CuCl_2$, and their concentrations were from 0.05 to 10 mol·m^{-3}. Before each measurement, the cell was kept still for 5 min to allow the membrane to equilibrate with the solution at the applied concentration, and after the measurement, the solution in the cell was changed to a higher concentration to perform another measurement, until the last one. All dielectric measurements were carried out at a temperature of 19−20 °C. The experiment was repeated three times, and the dielectric spectra obtained each time agreed with each other very closely. Theoretical analysis was then applied on a spectrum randomly chosen from them.

4. Results and Discussion

4.1. Characteristics of the Dielectric Spectra and Mechanism for the Behavior. Figure 2 shows the dielectric spectra, i.e., frequency (f) dependence of capacitance (C), and conductance (G) of the system composed of the NF membrane and LiCl solutions of various concentrations. The same data are plotted in a complex plan diagram (Figure 3). The spectra of the systems with solutions of other electrolytes had similar characteristics. It could be seen that, for the LiCl solution of any concentration, there were two remarkable dielectric relaxations in the studied frequency range: two distinct decrements (or increments) of capacitance (or conductance) are observed around certain frequencies, and a semicircle and a circular arc could be seen in the complex plan plot. These two relaxations showed different features when the environmental condition is changed.

To fully understand the characteristics of the dielectric spectra and their behavior, and also to probe into the reason for the relaxations, it is necessary to obtain the dielectric parameters characterizing the double relaxation. Therefore, we fitted the

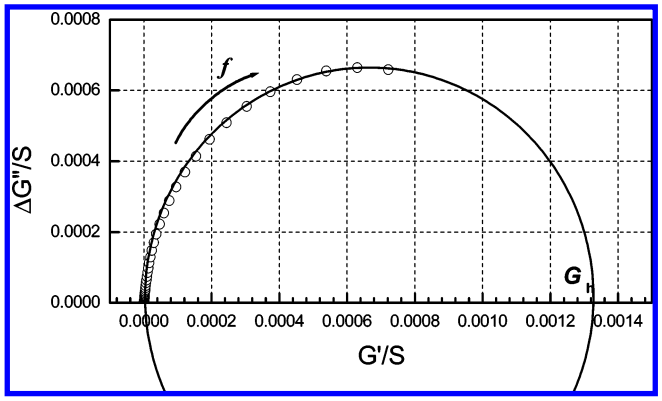

Figure 4. Determination of G_h in a Cole−Cole plot (also complex plan plot) of complex conductance for the system with a membrane in a 10 mol·m^{-3} LiCl solution. The intensity of the low-frequency relaxation was too small to appear in the plot at the present scale. The high-frequency relaxation is Debye type, and its Cole−Cole plot is a semicircle, theoretically. The abscissa value of the intersection of the semicircle tracing the experiment data with the abscissa axis is G_h, and $\Delta G'' = (C(f) - C_h)2\pi f$.

$C-f$ curves with a formula combining the Cole−Cole equation and the Debye equation to extract characteristic parameters from the $C-f$ curves:[9]

$$C(f) = \frac{(C_l - C_m)\left[1 + \left(\frac{f}{f_p}\right)^{1-\alpha}\cos\left(\frac{\pi}{2}(1-\alpha)\right)\right]}{1 + 2\left(\frac{f}{f_p}\right)^{1-\alpha}\cos\left(\frac{\pi}{2}(1-\alpha)\right) + \left(\frac{f}{f_p}\right)^{2(1-\alpha)}} + \frac{C_m - C_h}{1 + \left(\frac{f}{f_q}\right)^2} + C_h \quad (10)$$

where, C_h, C_m, and C_l are capacitance at the plateaus of the $C-f$ curve in the high-, middle-, and low-frequency range, respectively; f_p and f_q are characteristic relaxation frequencies of the low- and high-frequency relaxations, respectively; and α is the distribution coefficient of the relaxation time, which reflects the complexity of the system's inner structure.[9] The larger the value of α is, the broader is the distribution of relaxation time.

Because the Cole−Cole equation cannot give all parameters for relaxation of conductance, the characteristic parameters G_h, G_m, and G_l were determined directly from the curves of $G-f$. Similarly, G_h and G_l are limit conductance at high and low frequencies, and G_m is conductance at the middle plateau of the $G-f$ curves. As electrolyte concentration increased, the high-frequency plateau shifted out of the frequency range (Figure 2), therefore the value of G_h could only be determined in a Cole−Cole plot of the complex conductance, i.e., curve of $\Delta G'' - G'$, as shown in Figure 4.

As an example, the characteristic parameters determined for membrane−LiCl solution systems were listed in Table 1. It can be seen that, for the high-frequency relaxation, decrement of capacitance, ΔC ($=C_m - C_h$), was invariable when external concentration increased. Meanwhile, the characteristic frequency f_q and increment of conductance, ΔG ($=G_h - G_m$), depended linearly on the external concentration, as illustrated in Figure 5. These were evident characteristics of membrane−solution interfacial polarization,[16,29] which is caused by the accumulation of ions on membrane−solution interfaces.

On the other hand, the dependence of characteristic parameters of the low-frequency relaxation on the concentration of

TABLE 1: Characteristic Parameters of the Dielectric Spectra for Membrane in LiCl Solutions of Various Concentrations

c [mol·m^{-3}]	C_l [pF]	C_m [pF]	C_h[a] [pF]	G_l[b] [nS]	G_m [nS]	G_h [μS]	f_p [Hz]	f_q [kHz]	a	$C_m - C_h$ [pF]	$C_l - C_m$ [pF]
0.05	96.910 ± 0.461	78.657 ± 0.365	14.60	82.272	184.88	15.469	894.67 ± 21.08	37.975 ± 0.279	0.283 ± 0.012	64.06	18.253
0.07	107.16 ± 0.45	77.031 ± 0.390	14.60	62.456	197.25	18.528	712.04 ± 21.78	46.731 ± 0.257	0.340 ± 0.013	62.40	30.129
0.1	113.12 ± 0.56	78.144 ± 0.379	14.60	58.189	183.09	24.217	568.35 ± 20.03	60.196 ± 0.429	0.317 ± 0.013	63.54	34.976
0.2	118.45 ± 0.65	77.852 ± 0.344	14.60	61.946	252.83	36.889	748.32 ± 21.02	92.184 ± 0.681	0.330 ± 0.012	63.25	40.598
0.4	123.43 ± 0.53	77.374 ± 0.312	14.60	70.847	337.83	65.753	922.61 ± 22.1	165.85 ± 1.47	0.303 ± 0.011	62.77	46.056
0.7	129.38 ± 0.48	76.878 ± 0.307	14.60	77.203	444.99	107.07	1114.9 ± 24.8	272.49 ± 2.95	0.281 ± 0.010	62.28	52.502
1	133.29 ± 0.38	76.853 ± 0.285	14.60	83.351	574.03	153.74	1383.7 ± 25.8	391.58 ± 4.57	0.268 ± 0.009	62.25	56.437
2	133.62 ± 0.44	77.784 ± 0.298	14.60	94.028	710.89	295.00	1758.3 ± 35.7	741.29 ± 10.77	0.265 ± 0.010	63.18	55.836
4	137.55 ± 0.43	77.047 ± 0.304	14.60	106.29	847.67	568.00	1950.2 ± 49.2	1445.5 ± 29.4	0.245 ± 0.010	62.45	60.503
7	138.21 ± 0.43	75.983 ± 0.322	14.60	120.21	1092.6	966.00	2487.0 ± 64.8	2501.8 ± 77.7	0.244 ± 0.010	61.38	62.227
10	139.68 ± 0.44	75.983 ± 0.320	14.60	123.51	1365.7	1392.0	3103.8 ± 72.5	3605.7 ± 141.7	0.250 ± 0.010	61.38	63.697

[a] The parameter C_h was fixed when the C-f curves were fitted with eq 10, because the high-frequency plateau of the curves shifted out of the measured frequency range with the increasing electrolyte concentration (Figure 2a), therefore the values of C_h for systems with high concentrations could not be obtained accurately by fittings, but they tended to be equal to those found for the systems with low concentrations, i.e., 14.60 pF. The error was estimated to be 0.5% of the data. [b] The errors of G_l, G_m, and G_h were estimated to be below 0.5% of the data.

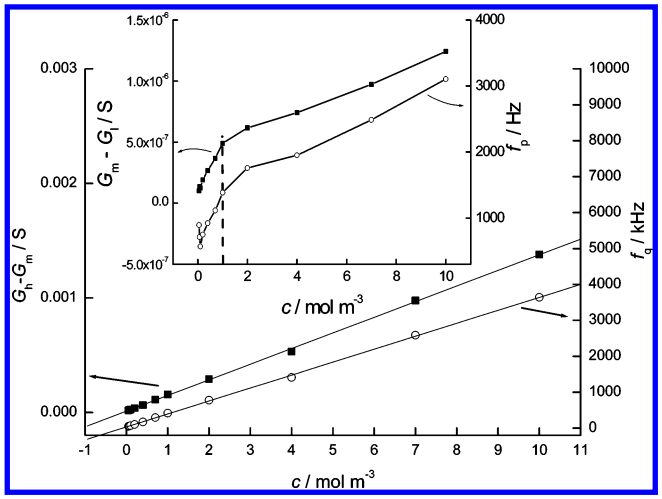

Figure 5. Increment of conductance, ΔG, and characteristic relaxation frequency, f_p or f_q, of the two relaxations vs external electrolyte concentration for systems with the membrane in LiCl solutions.

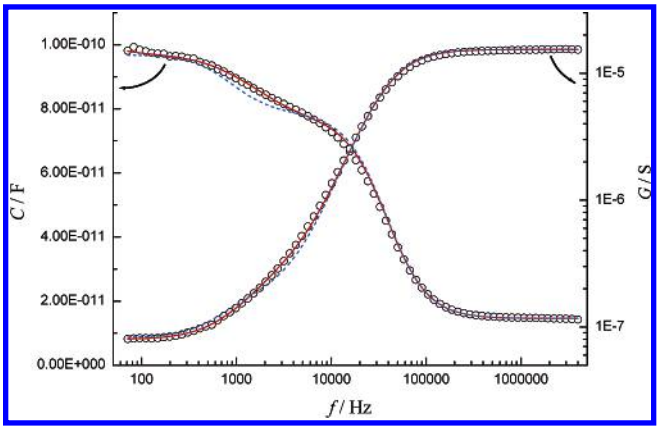

Figure 6. A comparison of two theoretical calculations with the experiment data (open circles), for the membrane in LiCl solution of 0.05 mol·m^{-3}. Dotted lines are the spectrum of the membrane−solution system calculated based on the simple three-phase model; solid lines are the best-fit curve with eqs 2−7.

the solution was different from that of the high-frequency relaxation. The amplitude of capacitance, $\Delta C'$ ($=C_l - C_m$), increased evidently with the increasing external concentration at low concentrations, whereas it increased slowly when the concentration was higher than 1 mol·m^{-3}, which was shown as underlined data in Table 1. Moreover, the curves of the increment of conductance ($\Delta G'$, equal to $G_m - G_l$) and the characteristic frequency (f_p) vs the external concentration (c) both had an inflection at the concentration of 1 mol·m^{-3}. The slopes at the two sides of this concentration were distinctly different, as shown in the inset in Figure 5. The complex variation of these characteristic parameters indicated that the influence of bulk concentration on the low-frequency relaxation was complicated and indirect.

There is an assumption recognized in dielectric studies: the bigger the structure of the dielectric, the larger the relaxation time (τ_0) and the smaller the relaxation frequency ($f_0 = 1/2\pi\tau_0$).[30] This allows us to consider that the membrane phase is the origin of the relaxation that occurred at the low frequency range because of its comparatively larger structure. Furthermore, since the high-frequency relaxation has been attributed to the interfacial polarization between membrane and solution, the low-frequency relaxation can be ascribed to the nonuniformity of the membrane inner structure. Therefore, we suggest that the membrane is composed of two layers with different electrical properties, which cause the low-frequency relaxation. Increasing bulk solution concentration changed the properties of the two layers, resulting in the change in the characteristic parameters of the low-frequency relaxation. The complex dependence of characteristic parameters on solution concentration implied that the two layers within the membrane responded to the environment differently. As can also be seen in Figure 2, the relaxation intensities in C and G at the low-frequency range become clearer gradually with the increase of the electrolyte concentration. It can be considered also that the difference between electric properties of the two layers was enlarged when the electrolyte concentration increased.

4.2. Dielectric Analysis. Since the dielectric spectra with two relaxations indicate that there are at least two interfaces in the system, we considered a simple three-phase model that has three homogeneous phases: one aqueous phase and two layers that correspond to the double layer structure in the membrane. This dielectric model is analogous to the one described in the theoretical discussions except that it does not consider the conductivity distribution of phase c. For this model, there has been a modeled analyzing method, with which phase parameters can be calculated through the characteristic parameters of the dielectric spectra.[17] The complex capacitance of the model is expressed by modified eq 7 with frequency independent C_c* instead of $C_c(f)$*. The calculated spectrum is shown in Figure 6 as dotted lines, which agreed with the experiment data at most frequencies, except at about 1000 Hz where the low-frequency relaxation occurred. In dielectric analysis, this tiny discrepancy can provide much information about membrane inner structure, and thus should not be ignored.

As discussed in subsection 2.2, the broadening of the low-frequency relaxation may be caused by heterogeneity in one of the two layers. Therefore, we improved the model by introducing a conductivity distribution of one layer in the membrane into the dielectric model described in the theoretical discussions. By using this model, the observed dielectric spectra were fitted with eqs 2, 3, and 7 by the least-squares method. The value of G_1 obtained from the fittings was lower than 10^{-7} S, but it was not able to be precisely determined because the dielectric spectra are not sensitive to G_1. Therefore, the value of G_1 was fixed, and the values of other phase parameters, C_b, G_b, C_c, and G_2, were obtained, as shown in Figures 7, 8, 9, and 11.The correlation coefficients between the experimental data and the theoretical curves were above 0.995. The fitted curves for the membrane in 0.05 mol·m^{-3} LiCl solution, as an example, were also shown in Figure 6, as the solid lines, which agreed much better with the experimental data at all frequencies.

4.3. Analysis of the Result: Identification of Membrane Layers and Electrical Properties of Each Layer. Figures 7 and 8 show the dependence of capacitance C_b and conductance G_b of phase b on the electrolyte concentration in different solutions. C_b increased with the increase of concentration c when c <1 mol·m^{-3}, and varied with different electrolytes at each applied concentration, indicating that the configuration of the polymeric material in phase b was dependent on the concentration and species of the electrolyte.

Compared with the conductance of phase c, especially on the side facing the solution, G_2 (Figure 9), G_b was smaller by 2 orders of magnitude, indicating that ions permeate through phase b with more difficulty. There are two possible reasons: phase b is thicker, or ion mobility in this phase is slower. Moreover, except in $MgCl_2$ and $BaCl_2$ solutions, G_b increased gradually with increasing bulk concentration. This could be attributed to increased free ions that entered the pores of the

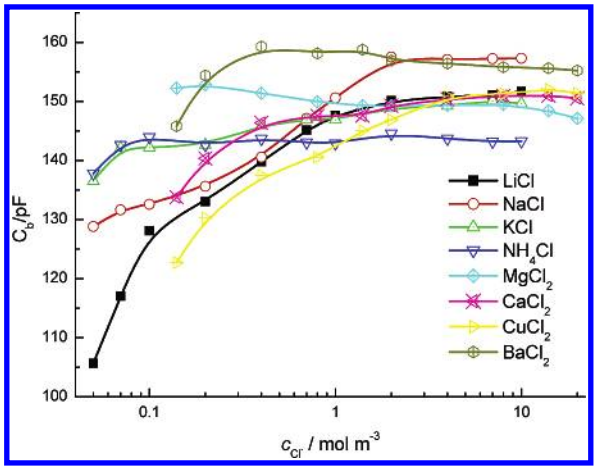

Figure 7. Capacitance C_b of phase b vs electrolyte concentration in different solutions.

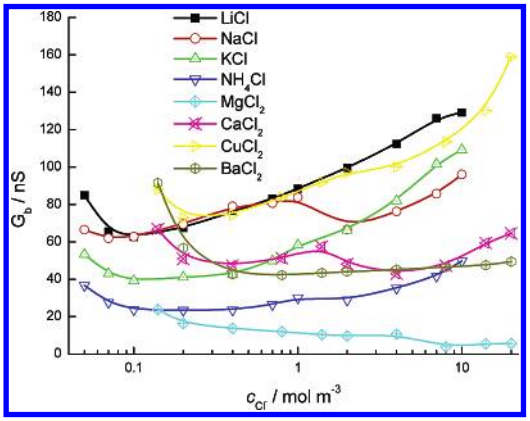

Figure 8. Conductance G_b of phase b vs electrolyte concentration in different solutions.

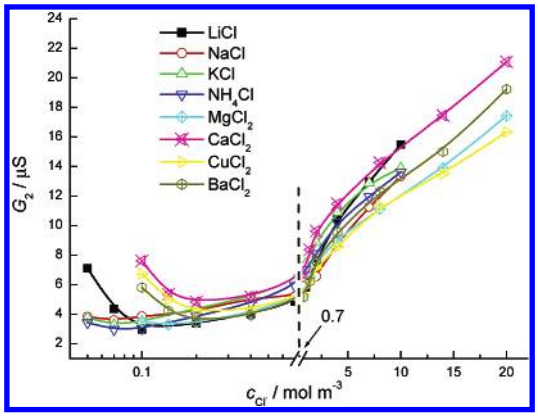

Figure 9. G_2 vs electrolyte concentration and species.

membrane. In addition, there were evident differences in G_b between different electrolytes. The values of G_b for monovalent cations were higher than those for divalent cations (except NH_4Cl and $CuCl_2$). This is an indication that the scale of pores in phase b is small enough to exhibit permselectivity on size and charge number of the ion, conforming to an essential characteristic of dielectric exclusion and steric hindrance: small pore size and low water content in the membrane cause dielectric exclusion; ions with more charges cause stronger polarization on the pore wall, thus undergoing stronger electrostatic repulsion force; ions with larger size are more likely to be blocked by the membrane polymers.[3]

Furthermore, in extremely dilute solutions, G_b decreased with increasing bulk concentration. This could be interpreted as follows: besides free ions of the applied electrolyte, there are H^+ ions in the membrane, which move faster than any other ions under most conditions. The other ions which penetrated into the membrane pores combine water molecules through hydration effect and thus intermit the transport of H^+, which depends on formation and rupture of hydrogen bonds with water molecules. As a result, the membrane conductivity decreases. This phenomenon only occurred in extremely dilute solutions because the concentration of H^+ was very small. At much higher concentrations, conductance would be dominated by other ions.

Figure 9 shows the electrolyte concentration dependence of G_2. The values of G_2 were between 3 and 20 μS and much higher than G_1, which was lower than 10^{-7} S. Thus, G_2 could be considered as twice the mean conductance of phase c, because the conductivity was linearly distributed according to the model (Figure 1). There was an inflection at about 0.7 mol·m^{-3} in Figure 9. Below 0.7 mol·m^{-3}, G_2 was almost independent of the electrolyte concentration, while above 0.7 mol·m^{-3}, G_2 increased linearly with increasing bulk concentration. This is an exhibition of Donnan equilibrium between solution and membrane with fixed charges. To keep electroneutrality of the membrane phase and equalize the electrochemical potential of the ions in the membrane and in the solution, the overall concentration of ions in the membrane is invariable when the bulk concentration is lower than the concentration of fixed charges in the membrane. Therefore in this concentration range, membrane conductivity remains constant. When the bulk concentration is higher than the concentration of the fixed charges, the effect of fixed charges disappears, because the charges are neutralized by counterions in the membrane. Coions and counterions then enter the membrane because of the concentration gradient, and thus membrane conductivity increases proportionally with the bulk concentration.

The interpretation for Figure 9 could be proved by theoretical calculation. In a previous paper, the authors had given the expressions of cation and anion's concentration in membrane under Donnan equilibrium, which were functions of bulk concentration and fixed charge density of the membrane.[16]

Membrane conductivity κ_m is related to concentration and mobility of free ions in the membrane, and the contribution of H^+ is also taken into account, so κ_m is expressed by:

$$\kappa_m = (U^m_{M^+} c^m_{M^+} + U^m_{A^-} c^m_{A^-} + U^m_{H^+} c^m_{H^+})F \qquad (11)$$

where, $U^m_{M^+}$, $c^m_{M^+}$, $U^m_{A^-}$, $c^m_{A^-}$, $U^m_{H^+}$, and $c^m_{H^+}$ denote mobility and concentration of cation, anion, and proton in the membrane, respectively. F is the Faraday constant, 96485 C. The expressions in ref 16 are used for $c^m_{M^+}$ and $c^m_{A^-}$ in eq 11. And combined with eq 9, the dependence of G_2 on the concentration c could then be calculated by introducing proper numerical values for unknown parameters in the expression. Figure 10 showed a rough simulation for the data of the membrane in NaCl solutions. The thickness of phase c was assumed to be 60 μm (for details see section 4.4).

The simulation gave the following: fixed charge density, 0.7 mol·m^{-3}; $U^m_{Na^+} + U^m_{Cl^-} = 2.0 \times 10^{-12}$ S·m^2·mol^{-1}·C^{1-}; and $U^m_{H^+} c^m_{H^+} \geq 7.2 \times 10^{-12}$ S·m^{-1}·C^{-1}. The value of $U^m_{Na^+} + U^m_{Cl^-}$, sum of the mobility of Na^+ and Cl^- in phase c, was obtained; then both the mobility of Na^+ and Cl^- in phase c were considered to be smaller than 2.0×10^{-12} S·m^2·mol^{-1}·C^{-1}. This value is 20 to 40 ppm of the ions' mobility in solution, which can be easily obtained from handbooks. On the other hand, if the concentration of H^+ was identical in membrane and in solution, $c^m_{H^+}$ should be 10^{-3} mol·m^{-3}, for the pH

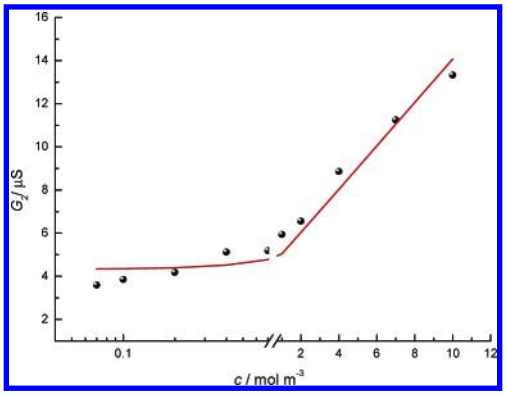

Figure 10. A rough simulation with Donnan equilibrium principle for concentration dependence of G_2 of the membrane in NaCl solutions. The continuous curve was generated by Donnan equilibrium principle, and the symbols were the result of the dielectric analysis.

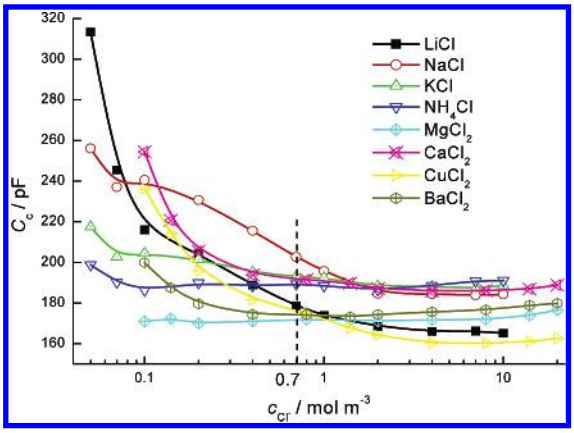

Figure 11. Apparent capacitance of phase c, C_c, vs bulk electrolyte concentration in different solutions.

was about 6. Then $U^{m}_{H^+}$ should be larger than 7.2×10^{-9} S·m^2·mol^{-1}·C^{-1} according to the simulation, which is 2% of H^+'s mobility in solution.

Theoretically, it should be noted, the concentration of H^+ in the membrane is not equal to that in the solution, because H^+ also obeys Donnan equilibrium. To describe the movement of ions, the above theoretical simulation was simplified, considering that the concentration of H^+ in solution is much smaller than that of the other ions.

Donnan exclusion prevents coions from entering membrane phase, but gives attraction on counterions. If distribution of ions is only controlled by Donnan exclusion, the overall concentration of ions in the membrane will be equal to that in solution when the bulk concentration is higher than the fixed charge concentration, and higher than that in solution when the solution is very dilute. However, the membrane phase is not infinitely loose, and the presence of polymers is bound to cause steric hindrance and dielectric exclusion on the ions, which decrease the concentration of ions in the membrane. Therefore in the simulation result, the distinct decrease of ion mobility in the membrane compared to that in solution actually contained two factors: decrease in ion concentration and in ion mobility. And the difference in the order of magnitude of ion mobility in membrane and in solution also showed that, besides Donnan exclusion, dielectric exclusion and steric hindrance also existed in this membrane layer.

In addition, we also learned from the simulation that H^+ underwent much less rejection than other ions in the membrane, as could be explained as follows: the other ions combined with hydrated water molecules have a larger size, and on the other hand, the way in which H^+ transports is different from that of other ions.

The simulation result and above discussions indicated that there were fixed charges in phase c, and their concentration at the side facing the solution was near 0.7 mol·m^{-3}. Therefore the polymeric material in phase c could be considered to be sulfonated polyether sulfone, in accordance with the literature where this polymer was reported to have negative fixed charges.[31] And the other layer of the membrane, phase b, was mainly composed of polyester.

Figure 11 showed the influence of electrolyte concentration and species on the apparent capacitance of phase c, C_c, which decreased gradually with the increasing bulk concentration at low concentrations and tended to be stabilized when the bulk Cl^- was above 0.7 mol·m^{-3}. It was seen clearly from the theoretical part that the way C_c varied with the solutions reflected the dependence of the permittivity ϵ_c on the solution, which was related to the property of the membrane material in phase c.

Since phase c is composed of sulfonated polyether sulfone with negative fixed charges, when the membrane was soaked in water, the polymer chains in this layer may keep as far away as possible from each other, because of the electrostatic repulsion effect between the fixed charges. When bulk electrolyte concentration increases, there would be more counterions in the membrane, and the electrostatic repulsion effect is gradually screened. As a result, the polymer chains may cluster. The change of gathering state of the polymers probably results in the change of membrane permittivity or capacitance. Moreover, after all the fixed charges have been screened by counterions, more ions would not cause any further changes in the polymer gathering state. Therefore, when the bulk Cl^- was above 0.7 mol·m^{-3}, the membrane capacitance was independent of the concentration, as shown in Figure 11.

4.4. Membrane Layer Thickness and Ion Transport Rate. To compare the transport rate of ions in both membrane layers and determine a clear detailed inner structure of the membrane, knowledge of membrane conductivity is required. However, because of the limitations of current measurement technology, the thickness of each membrane layer in the swollen state cannot be obtained. So we had to estimate the thickness of the layers by combining the capacitance and conductance data in analyzing the results.

The membrane−LiCl solution systems were taken as an example. The dielectric constant and conductivity of each membrane layer could be calculated by using the equation of $\epsilon = Ct/S\epsilon_0$ and eq 9, if the thickness t of both layers is known. If the thickness of phase b is smaller than 60 μm, $\overline{\epsilon_b}$, the mean of the dielectric constant of phase b, would be smaller than 3, the dielectric constant of dry polymers. This is certainly not reasonable, because there might be water in the membrane layer, and the dielectric constant should be larger than or at least equal to that of the dry polymers. This can be easily understood by seeing the empirical equation, $\epsilon_m = \epsilon_w f_w + \epsilon_d(1 - f_w)$, where ϵ_m, ϵ_w, and ϵ_d are dielectric constant of membrane, water, and dry polymers, respectively, and f_w is the water content in the membrane. Therefore, the thickness of phase b should be larger than 60 μm. Similarly, the thickness of phase c should be larger than 40 μm. Moreover, the whole membrane is 120 μm thick, therefore, the thickness of phase b should be between 60 and 80 μm, and that of phase c should be between 40 and 60 μm.

With the range of thickness of both membrane layers estimated above, the values of $\overline{\kappa_2}$ calculated are always larger

than those of $\overline{\kappa_b}$ by more than 50 times. This indicates remarkably that the pore size and water content in phase c are larger than those of phase b. Therefore, the dielectric constant of phase c, $\overline{\epsilon_c}$, should also be larger than that of phase b, $\overline{\epsilon_b}$. Then the thickness of phase b is restricted to be smaller than 70 μm, and the thickness of phase c should be larger than 50 μm; otherwise, the dielectric constant of phase c would be smaller than that of phase b. Thereby, we learned that the thicknesses of the two phases are close to each other, and ions can permeate through phase c more readily because of its larger pore size and water content.

We could look back into Figures 8 and 9: G_b, conductance of phase b, varied markedly when the bulk electrolyte species changed, whereas G_2, conductance of phase c at the side facing the solution, showed little difference for different electrolytes. This implies that pore size and water content in phase b are comparatively small, and great dielectric exclusion effect discriminates ions of different size and charge. Unlike phase b, phase c is much looser and its pore size is much bigger than that of the ions, and thus cannot discriminate different ions, although dielectric exclusion exists. In addition, because the electrolytes used in this work had the same anion (coion of the fixed charges), Donnan exclusion resulted in no permselectivity for these electrolytes. Hence, the conclusion on looseness and water content of each membrane layer could be justified simply by the results of the dielectric analysis. Thus we could conclude that ions transport in phase c more freely. However, it should be noted that phase c has already shown tremendous hindrance effect on ion permeation, as observed from the mobility ratios acquired in the simulation in Figure 10. Thereby, both layers in the membrane cause a hindrance effect for ion transport, only differing in degree and mechanisms.

5. Conclusion

By analyzing dielectric spectra of the membrane in electrolyte solutions, we draw the following conclusions. The double-layer structure of the membrane and interfacial polarization between the membrane and the solution cause the relaxation at low frequencies and high frequencies, respectively. Capacitance and conductance of the two membrane layers vary with external electrolyte concentration and species in a different manner. The two membrane layers have a similar thickness, but are different in the looseness or water content. Ions transport through these layers with different mobility and one of the layers shows permselectivity for different electrolytes.

Acknowledgment. The authors are grateful for the financial support of the National Natural Science Foundation of China (No. 20273010), and thankful to Dr. Ping Xu in Nitto. Denco. Co. for supplying the NF membrane specimen.

References and Notes

(1) Mohamed, N. A.; Al-Dossary, A. O. H. Structure−property relationships for novel wholly aromatic polyamide-hydrazides containing various proportions of para-phenylene and meta-phenylene units. III. Preparation and properties of semipermeable membranes for water desalination by reverse osmosis separation performance. *Eur. Polym. J.* **2003**, *39*, 1653−1667

(2) Lajimi, R. H.; Abdallah, A. B.; Ferjani, E.; Roudesli, M. S.; Deratani, A. Change of the performance properties of nanofiltration cellulose acetate membranes by surface adsorption of polyelectrolyte multilayers. *Desalination* **2004**, *163*, 193−202.

(3) Yaroshchuk, A. E. Dielectric exclusion of ions from membranes. *Adv. Colloid Interface Sci.* **2000**, *85*, 193−230.

(4) Bandini, S.; Vezzani, D. Nanofiltration modeling: the role of dielectric exclusion in membrane characterization. *Chem. Eng. Sci.* **2003**, *58*, 3303−3326.

(5) Khulbe, K. C.; Hamad, F.; Feng, C.; Matsuura, T.; Khayet, M. Study of the surface of the water treated cellulose acetate membrane by atomic force microscopy. *Desalination* **2004**, *161*, 259−262.

(6) Khayet, M. Membrane surface modification and characterization by X-ray photoelectron spectroscopy, atomic force microscopy and contact angle measurements. *Appl. Surf. Sci.* **2004**, *238*, 269−272.

(7) Ballinas, L.; Torras, C.; Fierro, V.; Garcia-Valls, R. Factors influencing activated carbon-polymeric composite membrane structure and performance. *J. Phys. Chem. Solids* **2004**, *65*, 633−637.

(8) Xu, T. W.; Hu, K. Y. A simple determination of counter-ionic permselectivity in an ion exchange membrane from bi-ionic membrane potential measurements: permselectivity of anionic species in a novel anion exchange membrane. *Sep. Purif. Technol.* **2004**, *40*, 231−236.

(9) Asami, K. Characterization of heterogeneous systems by dielectric spectroscopy. *Prog. Polym. Sci.* **2002**, *27*, 1617−1659.

(10) Zhao, K. S.; Asami, K.; Lei, J. P. Dielectric analysis of chitosan microsphere suspensions: study on its ion adsorption. *Colloid Polym. Sci.* **2002**, *280*, 1038−1044.

(11) Chen, Z.; Zhao, K. S. Dielectric analysis of macroporous anion-exchange resin beads suspensions. *J. Colloid Interface Sci.* **2004**, *276*, 85−91.

(12) Sancho, M.; Martínez, G.; Martín, C. Accurate dielectric modelling of shelled particles and cells. *J. Electrost.* **2003**, *57*, 143−156.

(13) Oleinikova, A.; Sasisanker, P.; Weingä1rtner, H. What can really be learned from dielectric spectroscopy of protein solutions? A case study of Ribonuclease A. *J. Phys. Chem. B* **2004**, *108*, 8467−8474.

(14) Srikhirin, T.; Schuele, D. E.; Mann, J. A., Jr.; Lando, J. B. Application of Dielectric Relaxation Spectroscopy to Ultrathin Langmuir−Blodgett Films. *Macromolecules* **2000**, *33*, 2584−2594.

(15) Zhao, K. S.; Yasuhiro, M.; Asaka, K.; Asami, K.; Hanai, T. Dielectric analysis of concentration polarization phenomena at cation-exchange membrane−solution interfaces by frequency variation and d.c. bias application. *J. Membr. Sci.* **1991**, *64*, 163−172.

(16) Li, Y. H.; Zhao, K. S. Dielectric analysis of nanofiltration membrane in electrolyte solutions: influences of electrolyte concentration and species on membrane permeation. *J. Colloid Interface Sci.* **2004**, *276*, 68−76.

(17) Kiyohara, K.; Zhao, K. S.; Asaka, K.; Hanai, T. Determination of capacitance and conductance of the constituent phase from dielectric observations on terlamellar composite systems. *Jpn. J. Appl. Phys.* **1990**, *29*, 1751−1756.

(18) Osaki, T.; Tanioka, A. Dielectric relaxation on the intermediate layer in a bipolar membrane under the water splitting phenomenon. I. Shift of the dielectric properties by means of time-dependent impedance measurements II. Double dielectric relaxation and identification of phase parameters. *J. Colloid Interface Sci.* **2002**, *253*, 88−93, 94−102.

(19) Chilcott, T. C.; Chan, M.; Gaedt, L.; Nantawisarakul, T.; Fane, A. G.; Coster, H. G. L. Electrical impedance spectroscopy characterisation of conducting membranes. I. Theory; II. Experimental. *J. Membr. Sci.* **2002**, *195*, 153−167, 169−180.

(20) Coster, H. G. L.; Chilcott, T. C.; Coster, A. C. F. Impedance spectroscopy of interfaces, membranes and ultrastructures. *Bioelectrochem. Bioenerg.* **1996**, *40*, 79−98.

(21) Coster, H. G. L.; Chilcott, T. C. *Surface Chemistry and Electrochemistry of Membranes*; Sørensen, T. S., Ed.; Marcel Dekker: New York, 1999; pp 749−792.

(22) Maxwell, J. C. *Treatise on electricity and magnetism*; Clarendon Press: Oxford, UK, 1891.

(23) Wagner, K. W. Erklärung der dielektrishen Nachwirkungsvorgänge auf Grund Maxerllsher Vorstellungen. *Arch. Elektrotech.* (*Berlin*) **1914**, *2*, 371−387.

(24) Hanai, T.; Zhang, H. Z.; Sekine, K.; Asaka, K.; Asami, K. The number of interfaces and the associated dielectric relaxations in heterogeneous systems. *Ferroelectrics* **1988**, *86*, 191−204.

(25) Asaka, K. Dielectric properties of cellulose acetate reverse osmosis membranes in aqueous salt solutions. *J. Membr. Sci.* **1990**, *50*, 71−84.

(26) Zhao, K. S. Asaka, K.; Asami, K.; Hanai, T. Theory and observation of dielectric relaxation due to the interfacial polarization for terlameller structure. *Bull. Inst. Chem. Res., Kyoto Univ.* **1989**, *67*, 225−255.

(27) Hanai, T.; Zhao, K. S.; Asaka, K.; Asami, K. Dielectric theory of concentration polarization. Relaxation of capacitance and conductance for electrolyte solutions with locally varying conductivity. *J. Membr. Sci.* **1991**, *64*, 153−161.

(28) Hanai, T.; Zhao, K. S.; Asaka, K.; Asami, K. Theoretical approach and the practice to the evaluation of structural parameters characterizing concentration polarization alongside ion-exchange membranes by means of dielectric measurement. *Colloid Polym. Sci.* **1993**, *271*, 766−773.

(29) Hanai, T. *Membrane* **1989**, *14*, 101.

(30) Ermolina, I.; Lewis, A.; Feldman, Y. Dielectric Properties of the bR membrane. *J. Phys. Chem. B* **2003**, *107*, 14537−14544.

(31) Benavente, J.; Cañas, A.; Ariza, M. J.; Lozano, A. E.; de Abajo, J. Electrochemical parameters of sulfonated poly(ether ether sulfone) membranes in HCl solutions determined by impedance spectroscopy and membrane potential measurements. *Solid State Ionics* **2001**, *145*, 53−60.